Available online at www.sciencedirect.com

ScienceDirect

Journal of the European Ceramic Society 35 (2015) 153–161

www.elsevier.com/locate/jeurceramsoc

Electrical behavior analysis of n-type $CaCu_3Ti_4O_{12}$ thick films exposed to different atmospheres

M.A. Ponce [a], M.A. Ramirez [b,*], F. Schipani [a], E. Joanni [c], J.P. Tomba [a], M.S. Castro [a]

[a] *Institute of Materials Science and Technology (INTEMA), University of Mar del Plata (UNMdP), National Research Council (CONICET), Av. Juan B. Justo 4302, (B7608FDQ) Mar del Plata, Argentina*

[b] *Faculdade de Engenharia de Guaratinguetá, Universidade Estadual Paulista, UNESP, Av. Ariberto Pereira da Cunha, 333, CEP: 12516-410 Guaratinguetá, SP, Brazil*

[c] *CTI Renato Archer, Rodovia D. Pedro I (SP - 65) Km 143,6, CEP: 13069-901 Campinas, SP, Brazil*

Received 25 June 2014; received in revised form 25 August 2014; accepted 28 August 2014

Available online 12 September 2014

Abstract

In this work n-type $CaCu_3Ti_4O_{12}$ (CCTO) thick films obtained by screen printing were studied. The role of the potential barrier characteristics (height and width) was considered in order to explain the electrical behavior. The electrical response was also analyzed considering the oxygen adsorption and subsequent diffusion into the grains at temperatures higher than 280 °C. Tunnel currents were also calculated taking into account the donor concentration values for films in vacuum atmosphere.

Published by Elsevier Ltd.

Keywords: Semiconductor; Conduction mechanism; $CaCu_3Ti_4O_{12}$; Diffusion

1. Introduction

Semiconductor metal oxides have been proven to be excellent in important characteristics such as sensitivity, long-term stability, robustness and price in the field of gas sensing. The detection of several gases can be performed by measuring changes in the electrical conductivity of films or bulk samples.[1–4] For all oxide semiconductors oxygen can be chemisorbed at grain surfaces as charged species, affecting intergranular potential barriers that control the conductivity.[5–10] Thus, the sensing mechanism is mainly based on surface reactions involving chemisorbed species.[7–11]

$CaCu_3Ti_4O_{12}$ (CCTO)-based ceramics are well known for their colossal dielectric constant (CDC) phenomenon that remains a topic of great scientific interest.[12–19] Based on the CDC properties, CCTO-based films might offer great advantages for electronic applications. By using impedance spectroscopy, Sinclair et al.[16] concluded that CCTO ceramics are composed of semiconductor grains and insulating grain boundaries. They attributed the CDC phenomenon to the existence of an internal barrier layer capacitance. On the other hand, Muralt et al.[14] have found evidence of a metal–insulator–semiconductor (MIS) junction formed at the electrode interface and the high capacitance value of CCTO samples was attributed to this junction. Bueno et al.[20] proposed another model which explains the unusually high dielectric constant and considered that an internal barrier layer capacitance mechanism is responsible for this phenomenon. In this model, barriers operate in the nanoscale range due to polaron defects associated to stacking faults. This mechanism is referred to by the authors as Nanoscale Barrier Layer Capacitance (NBLC).

As mentioned in previously published papers, p-type conductivity was observed in CCTO films tested at room temperature.[13–15] p-Type conduction at higher temperatures has been confirmed in CCTO films obtained by using RF-sputtering.[17] However, CCTO films may contain more than one

* Corresponding author.
E-mail address: margbrasil@yahoo.com (M.A. Ramirez).

http://dx.doi.org/10.1016/j.jeurceramsoc.2014.08.041
0955-2219/Published by Elsevier Ltd.

type of defect with different energy levels. N-type behavior has also been observed in CCTO films.[12] Through nanoscopic dielectric investigations, it was demonstrated that CCTO films grown by metal organic chemical vapor deposition on $LaAlO_3$ substrates possess n-type semiconducting nature.[21] Thus, p- or n-type conductivity strongly depends on processing characteristics.[12,18,19] Chung et al.[18] have found the presence of Schottky potential barriers at CCTO grain boundaries. These potential barriers act as obstacles to the current flow in polycrystalline ceramics, and were assigned as responsible for the non-ohmic behavior.[22,23] In n-type gas sensors, oxidizing gases decrease the conductivity while the exposure to reducing gases results in a lower coverage of oxygen, with the electrons returning to the grains and decreasing the barriers. However, native point defects, vacancies and interstitials can be influenced by gas adsorption affecting the semiconductor properties. This phenomenon can be used to improve the gas sensitivity.[7]

In this work, basic mechanisms related to the dependence of the surface barriers in CCTO exposed to different atmospheres were studied. The n-type semiconductor behavior of CCTO was analyzed considering the influence of a spurious CuO phase at the grain boundaries. Modifications in oxygen vacancy concentration under different atmospheres were also considered.

2. Experimental procedure

$CaCu_3Ti_4O_{12}$ (CCTO) powders were prepared by solid state reaction. Stoichiometric amounts of TiO_2 (Aldrich, 99.9%), CuO (Aldrich, 99.9%) and $CaCO_3$ (Aldrich, 99.99%) were ball milled in isopropyl alcohol in a polyethylene bottle using zirconium oxide balls. The powders were milled for 24 h in order to obtain a homogeneous mixture with reduced particle size. After isopropyl alcohol evaporation, the resulting powder was mechanically disaggregated in a mortar and sieved using a 200 mesh sieve. Afterwards, the materials were heated at 900 °C for 12 h in a conventional furnace using a heating rate of 5 °C/min. Thick films were prepared by the screen printing method. First, silver electrodes (interdigitals paths of approximately 1 mm) were deposited on a dense alumina substrate using a silk screen mask. The electrodes were thermally treated at 350 °C for 30 min using a heating rate of 5 °C/min. In the slurry preparation for obtaining CCTO thick films, 60 mg of CCTO powder and 2 drops of glycerin were mixed in a mortar. The viscosity of the mixture was controlled by dilution with isopropyl alcohol. Afterwards, this slurry was deposited on the electrodes with a glass rod. In order to evaporate the organic binder and to improve the adhesion of films to the alumina substrate, they were thermally treated at 60 °C for 1 h and then at 500 °C for 1 h, in both cases using a heating rate of 5 °C/min under vacuum (10^{-4} mmHg). The resulting film thickness was around 100 μm. Crystalline phases were analyzed by means of X-ray diffraction (XRD) recorded on a RIGAKU RINT2000 (42 kV/120 mA) diffractometer, with CuKα radiation in the 2θ range from 20° to 80° and a scan rate of 0.02°/min. Raman spectra were acquired at room temperature with a Renishaw inVia Reflex confocal microscope with a 514 nm excitation line (50 mW nominal power), via a 50X (0.75 NA) Leica metallurgical objective and a diffraction grating of 2400 lines/mm. The thick film morphology was assessed by scanning electron microscopy (Zeiss-Supra35 equipped with a field emission gun, SEM-FEG). Finally, the electrical behavior of films was analyzed using a multimeter (Agilent 34401A). For the resistance vs temperature cycling experiments, measurements were carried out while raising and then decreasing the temperature of the samples in the range 25–425 °C at a rate of ∼2 °C/min with the sample kept in vacuum (10^{-4} mmHg), dry air (760 mmHg) and CO (760 mmHg). Resistance vs time measurements were carried out in order to obtain curves under an air atmosphere. The resistance vs time measurements were performed in the range 250–400 °C, after a change of the atmosphere from vacuum (10^{-4} mmHg) to dry air (9.0 mmHg).

3. Results and discussion

In Fig. 1, the X-ray diffraction patterns of as-synthesized CCTO powders (a) and thick films (b) are shown. In both cases, the diffraction peaks can be indexed by a cubic body-centered perovskite-related structure according to JCPDS 75-2188 where all planes were indexed and the presence of small amounts of oxide cupper according to JCPDS 45-937. Fig. 1(c) shows a typical Raman spectrum of CCTO films. Major peaks at 443 and 509 cm^{-1}, which are associated with the Ag symmetry (TiO_6) rotation-like, along with a weak signal at 579 cm^{-1} attributed to the Ti–O–Ti antistretching mode of the TiO_6 octahedra are a characteristic signature of CCTO.[24] The Raman line observed at 754 cm^{-1} can result from the symmetric stretching breathing of the TiO_6 octahedra[24,25] Well-defined Raman peaks characteristic of CuO located at 285 cm^{-1}, attributed to the Raman active optical-phonon Ag mode of monoclinic CuO, and the weaker peaks at 346 and 618 cm^{-1}, assigned to Bg(1) and Bg(2) modes, respectively, can also be seen.[26,27] Also, traces of TiO_2 (anatase phase) are detected from peaks at 399, 639 cm^{-1} corresponding to Bg(1), and Eg modes, respectively.[28] Weak signals at 221 and 242 cm^{-1} can be assigned to the O–Ti–O bending mode in $CaTiO_3$.[29]

From SEM characterization of films surfaces, shown in Fig. 2, a porous microstructure composed of a relatively wide distribution of grain sizes was noticed (200 nm to 1 μm, Fig. 2a). By cross-section examination, it was determined that the film thickness was approximately 100 μm (Fig. 2b).

Fig. 3 shows the CCTO thick film conductance (G) as a function of temperature. Curves were acquired during a series of cycles obtained by increasing and decreasing the temperature in three different atmospheres. For samples in vacuum, (cycle a, points A–B–C), the final conductivity in the cooling process (point C) is higher than in the heating process. After this sequence, samples were exposed to air (cycle b, points D–E–F) and a decrease in sample conductivity was observed (point E). Moreover, after the cooling process, the sample conductivity was lower (point F). After the air cycle, the samples were exposed to CO (cycle c, points G–H–I) atmosphere and exhibited a higher conductivity after the complete cycle (point I).

In Fig. 4, the time response of the CCTO film is presented. Resistance was measured when samples heated in vacuum were

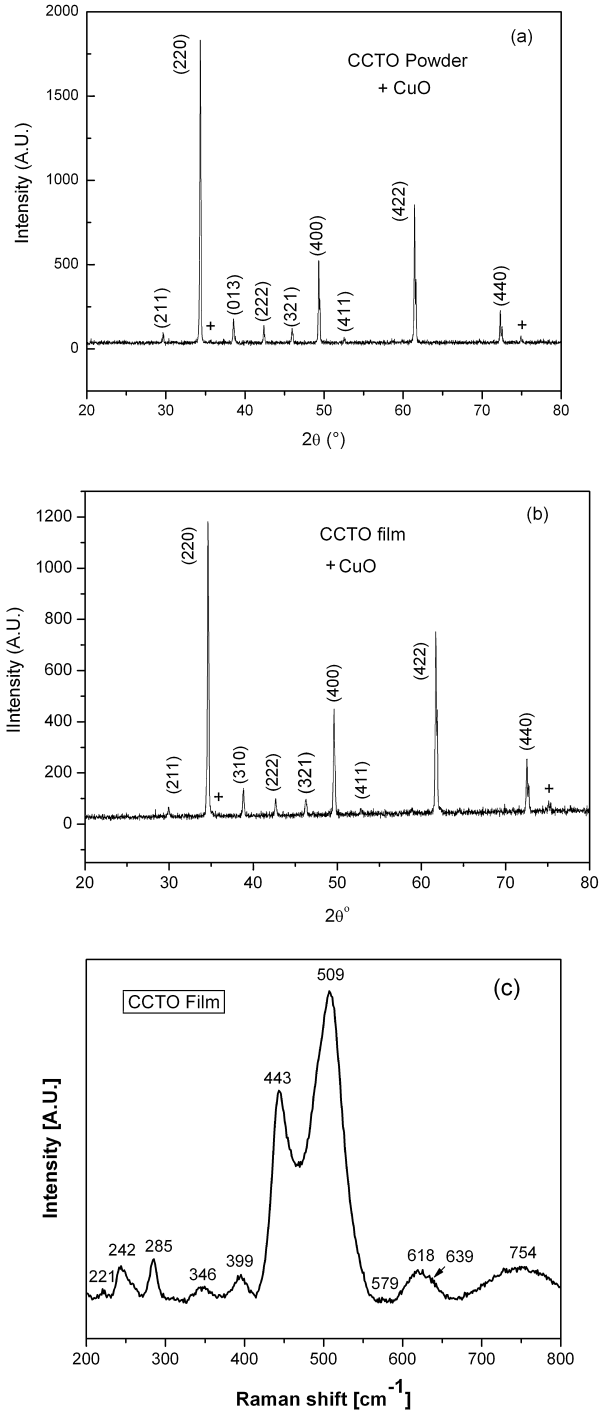

Fig. 1. X-ray diffraction patterns of as-synthesized CCTO powders (a) and thick films (b). Thick film Raman spectrum (c).

exposed to dry air at different temperatures (275 °C, 350 °C and 400 °C). In experiments carried out at the lower temperatures (275 and 350 °C), after a quick increasing due to air exposure, the electrical resistance remained almost constant. On the other hand, for temperatures close to 400 °C a decrease in the resistance after a quick increase was observed. In both cases the resistance decreases after the air removal.

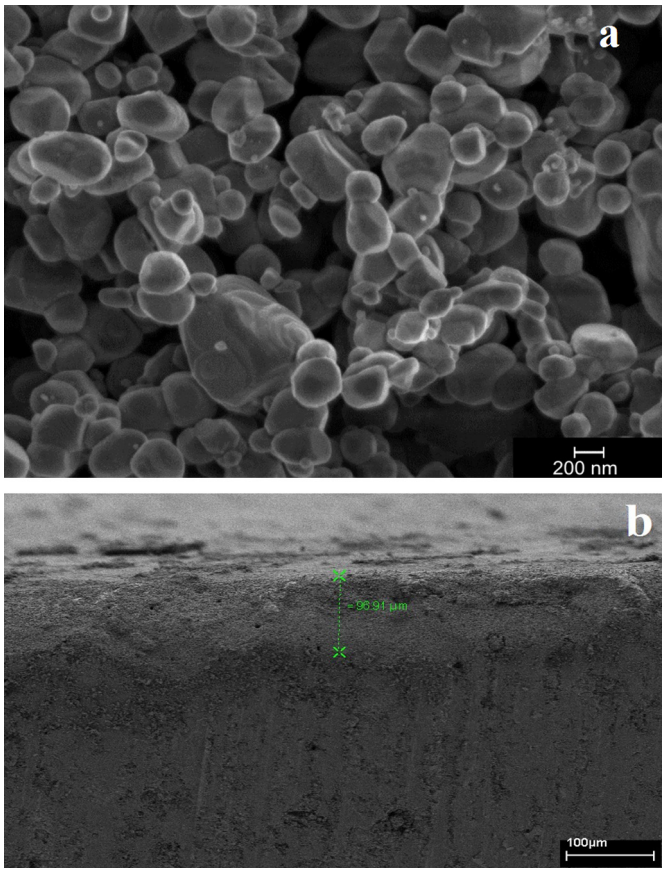

Fig. 2. SEM–FEG image of $CaCu_3Ti_4O_{12}$ thick films showing a typical surface morphology (a) and the film cross-section (b).

3.1. The presence of CuO at grain boundaries and semiconducting behavior

It is well-known that thermal treatments usually lead to an increase in film crystallinity with a consequent increase in surface stability. It has also been reported that intergranular potential barriers depend on the metal atoms segregated at the

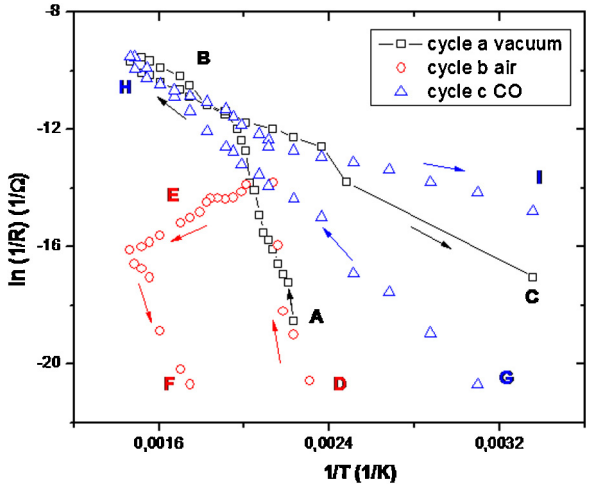

Fig. 3. CCTO thick film conductance (G) as a function of temperature in different atmospheres when the temperature is increased and decreased.

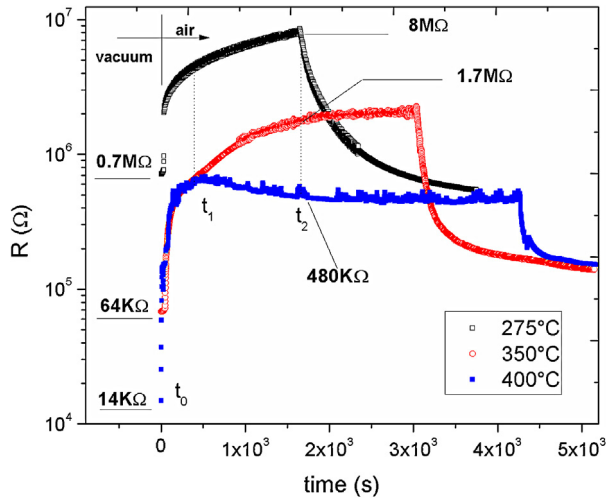

Fig. 4. Resistance vs. time curves of CCTO thick films for dry air at different temperatures (275 °C, 350 °C and 400 °C).

grain boundaries, especially Cu^{2+}.[30] Moreover, segregation of copper oxide at the grain boundaries was considered responsible for the high resistance associated with the grain boundary.[31–35] On the other hand, Yeoh et al.[32] observed that samples with higher amounts of CuO segregated at the grain boundaries exhibited lower dielectric constants when compared to samples having less CuO segregation.

Deng and Muralt[13] related the p-type behavior to a possible reaction taking place during synthesis and annealing of CCTO ceramics

$$4Cu_{Cu} + O_{latt} \leftrightarrow 4Cu'_{Cu} + \frac{1}{2}O_2 + V_O^{2+} + 2h^+ \quad (1)$$

where, Cu_{cu} are the Cu (II) ions in the lattice, O_{latt} corresponds to the oxygen in the lattice, Cu'_{Cu} are the Cu (I) ions in the lattice, V_O^{2+} and h^+ are the doubly ionized oxygen vacancies and holes, respectively. Through XPS analysis, Foschini et al. determined that Cu(I) is present in the CCTO crystalline structure as a point defect substituting Cu (II) and forming Cu'_{Cu} structural imperfections.[36]

During the synthesis procedure at high temperatures or low oxygen pressures, the Cu'_{Cu} species are favored and the reaction goes to the right, creating oxygen vacancies and holes, thus increasing the p-type character. At intermediate temperatures Cu'_{Cu} is the principal ion and oxygen in the environment forces the equilibrium to move to the left, reducing the concentration of oxygen vacancies, thus decreasing the p-type character.[37,38]

Furthermore, copper vacancies (V''_{Cu}) could be formed, due to the presence of the spurious phase (CuO) with the consequent Cu'_{Cu} formation, according to:

$$Zero \leftrightarrow V''_{Cu} + 2Cu^+_{Cu} \quad (2)$$

The origin of n-type semiconductivity in CCTO has also been attributed to the presence of Cu^+_{Cu} ions, explaining the conduction in CCTO ceramics through charge carriers hopping between Cu_{cu} and Cu^+_{Cu}.[19] In our samples, the n-type behavior can be related with the electrical resistance increase when samples are exposed to an oxidizing atmosphere. Indications of the presence of a secondary CuO phase, as revealed by minor but detectable peaks in Raman spectrum, are certainly consistent with the observed semiconducting behavior.

3.2. Oxygen adsorption, desorption and diffusion

As it was previously mentioned, n-type semiconducting behavior can be related to the presence of CuO at the grain boundary surfaces. When n-type films are exposed to an air atmosphere (with oxygen adsorption on their surfaces), the intergranular barriers are affected by changing their heights and widths.[37–40] Also, oxygen diffusion into the grains of n-type CCTO films should be considered, as discussed by Zhang et al.[37]

In this work it is assumed that oxygen is chemisorbed on the grain surfaces, increasing the barrier height and width. This is a fast process, so the equilibrium with atmospheric oxygen is reached rapidly. Subsequently, in a second process, oxygen diffuses slowly into the grains, annihilating oxygen vacancies and reducing the donor concentration. For the sake of simplicity, we will consider that the main adsorbed oxygen species on the CCTO surface are O'_{ads}, so the relevant reactions are reduced to:

$$\frac{1}{2}O_2(g) + S \leftrightarrow O^0_{ads} \quad (3)$$

$$O^0_{ads} + e^- \leftrightarrow O'_{ads} \quad (4)$$

where, S denotes a surface site, e^- is an electron, and O_2 an oxygen molecule in the gas phase.

Adsorbed oxygen leaves its site creating a doubly ionized interstitial,

$$O'_{ads} + e^- \leftrightarrow O''_{int} + S \quad (5)$$

Interstitial oxygen migrates from the surface to the bulk annihilating oxygen vacancies:

$$V_O^{2+} + O''_{int} \leftrightarrow O_{latt} \quad (6)$$

All the reactions are in equilibrium and the concentrations of the species involved depend on the partial pressure of oxygen present in the gas phase.

Fig. 5 shows a diagram with the basic mechanisms taking place at the CCTO surface in contact with an oxygen atmosphere. All the oxygen species appearing in Eqs. (3)–(6) are present. At the surface it is considered that oxygen adsorbs in the atomic form and desorbs as oxygen molecules. Oxygen adsorbed on the surface diffuses into the grain as interstitials. Oxygen may also diffuse out of the grain to be incorporated at the surface. Finally, oxygen vacancies and oxygen interstitials recombine to generate oxygen in the lattice.

3.3. Conduction mechanisms

It is generally accepted that barriers formed between grains are responsible for changes in sensor conductivity.[11,13,38–43] As a first approach to barrier height calculations, researchers have

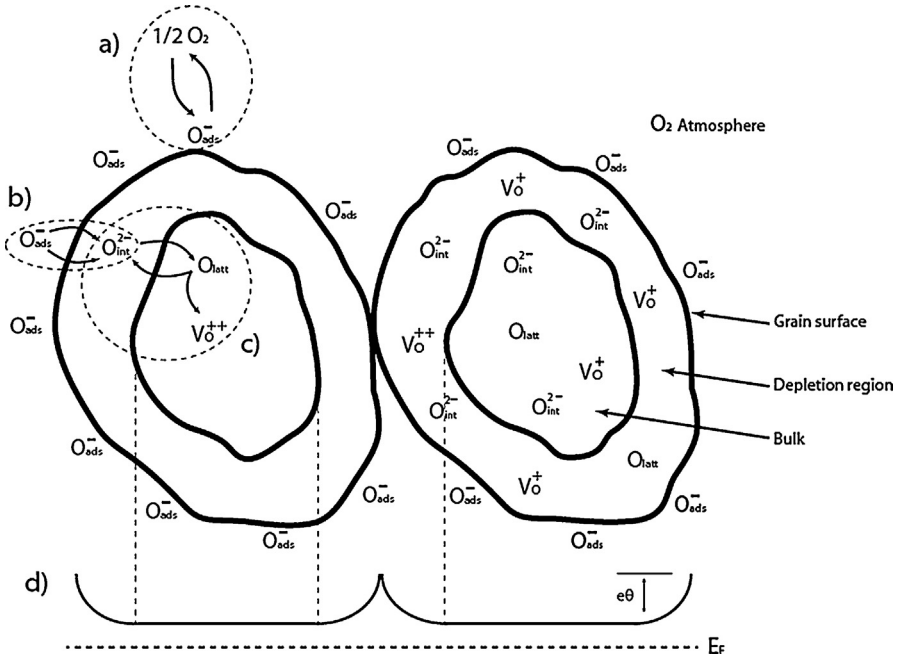

Fig. 5. Basic mechanisms in CCTO oxide sensors. (a) Oxygen exchange equilibrium between the atmosphere and the grain surface. (b) Diffusion of oxygen in and out of the grains. (c) Interstitial-vacancy creation and recombination. (d) Energy band diagram.

regularly considered only the thermionic conductivity (G) of n-type semiconductors[12–18]:

$$G = G_0 \exp\left(\frac{-\phi}{kT}\right) \tag{7}$$

where, ϕ is the barrier height, T the temperature and k the Boltzmann constant.

Eq. (7) reflects an activated process due to intergranular barriers. On other hand, Eq. (3) shows that as the oxygen concentration increases, there will be a larger amount of chemisorbed oxygen, which increases the potential barrier height and decreases the film conductivity, as Eq. (7) indicates.

The potential barrier height and donor concentration (N_d) are directly related as follows:

$$\phi = \frac{q^2 N_s^2}{2\varepsilon_r \varepsilon_0 N_d} \tag{8}$$

where, N_s represents the number of electrons (per unit of area) extracted from the depleted surface region Λ, ε_0 is the vacuum permittivity, ε_r the relative permittivity, and q the electron charge. The usual Schottky relation between ϕ and Λ can be obtained from Eqs. (8) and (9), considering that in an n-type semiconductor with a double Schottky barrier $2N_d = N_s$. Then, Λ can be deduced from Eq. (9) as follows:

$$\Lambda = \left[\frac{2\varepsilon_0 \varepsilon_r \phi}{qN_d}\right]^{1/2} \tag{9}$$

At this point it is important to note that the depletion layer region has been measured at the barrier bottom. In the case of CCTO, the ε_r reported values range from 100 to 5000. Such great difference affects directly the depletion layer heights and widths as shown in Eqs. (8) and (9).[43]

Fig. 3 shows the conductivity as a function of temperature for measurements performed on different gases. When the CCTO film was heated in vacuum, adsorbed oxygen on the grain surface desorbed, decreasing the barrier height and increasing the electrical conduction. In fact, after cooling down the initial resistance value was not recovered (point C in Fig. 3).

When temperature was increased, oxygen desorption and diffusion out of the grain (according to Eqs. (3)–(6)) are the two processes responsible for the resistance diminution. In this case the oxygen out-diffusion promotes the generation of oxygen vacancies, forcing the equilibrium in Eq. (6) to move to the left. This process increases the donor concentration of the n-type semiconductor and the depletion layer becomes thinner (Eq. (9)). The band model for grains exposed to vacuum (Fig. 3) during the cycle A–B–C is shown in Fig. 6A. The Schottky barrier height (ϕ) decrease is shown in the band model. After oxygen diffusion out of the grain, Fig. 3A point C, oxygen vacancy concentration is increased; the depletion width of intergrain barriers becomes narrower while the barrier heights decrease.

When CCTO films were exposed to an air atmosphere (in 25–425 °C range, Fig. 3 cycle b) during the heating and cooling processes, a different electrical response was observed with respect to the regular film behavior. During the first part of heating in air atmosphere (less than 200 °C), a decrease in resistance with increasing temperature was observed. This typical response for films based on semiconductor oxides, being caused by an improvement in the current transport mechanisms at higher temperatures. On the other hand, above 200 °C, an anomalous behavior occurred, since an increase of the electrical resistance was observed during the heating process. This anomalous response is related to the oxygen adsorption at the grain surfaces, increasing the barrier height. An even more important role in the conductance decrease is played by oxygen diffusion into the

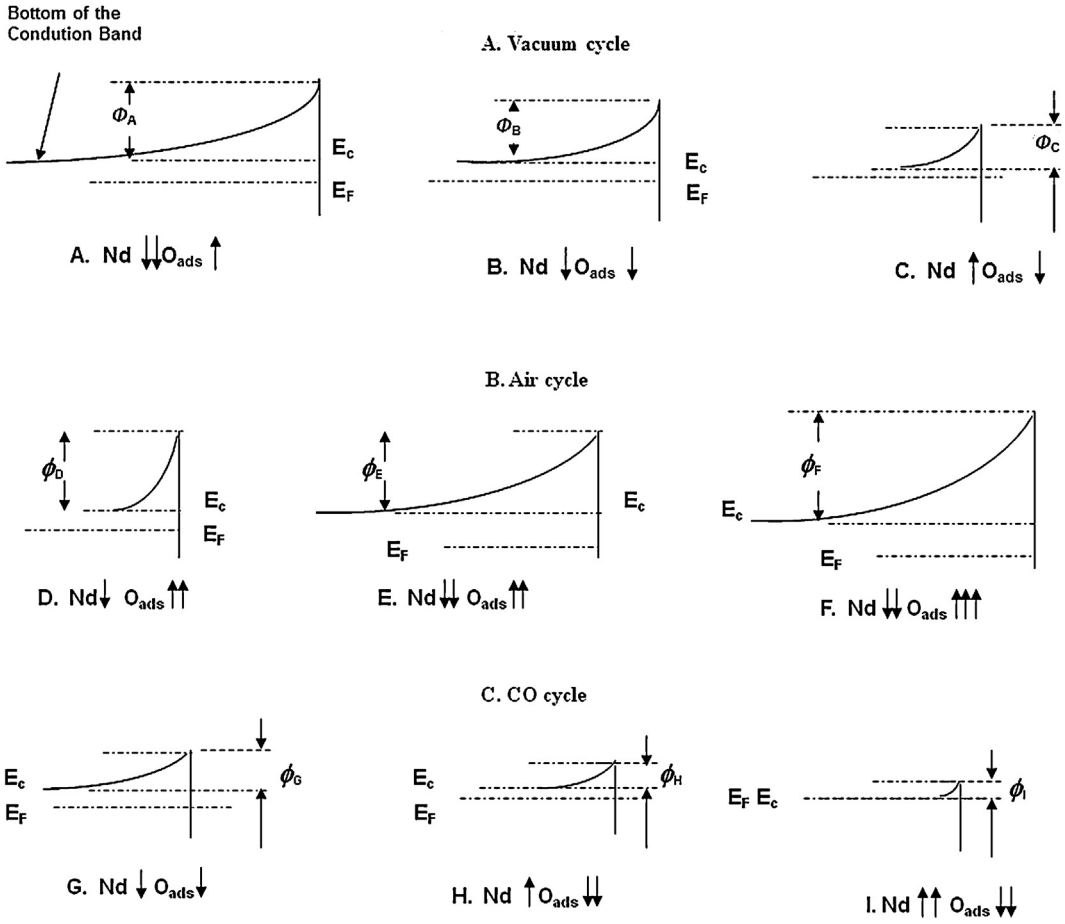

Fig. 6. Band diagrams for samples exposed to vacuum (A), air atmosphere (B) and CO atmosphere (C).

CCTO grains. This phenomenon annihilates oxygen vacancies generated in the previous treatment in vacuum atmosphere, forcing the equilibrium in Eq. (6) to move to the right. During the heating process in air, above 220 °C, barrier height modification occurs (changes in ϕ in Eq. (7)) and the barrier width increases as a consequence of oxygen in-diffusion (changes in Λ in Eq. (9) as a consequence of ϕ and N_d changes). In Fig. 6B, the band model for grains exposed to an air atmosphere (during the cycle D–E–F in Fig. 3), is also shown.

When films are exposed to a carbon monoxide atmosphere, this gas reacts with oxygen previously adsorbed on the CCTO film surface according to the subsequent equations:

$$O^-_{ads} + CO(g) \rightarrow CO_{2,ads} + e' \quad (10)$$

$$CO_{2,ads} \leftrightarrow CO_2(g) + S \quad (11)$$

This reduction in surface oxygen improves the sample conductivity.

It is generally accepted that oxygen vacancies in semiconducting oxides act as electron donors, so they tend to increase the conductivity of the n-type films. The band model for grains exposed to CO, during the cycle G–H–I in Fig. 3 is shown in Fig. 6C in which Schottky barriers of height ϕ at the grain surfaces determine the sample conductivity. After oxygen diffusion out of the grains, Fig. 6C, oxygen vacancy concentration is increased; the depletion width of intergrain barriers becomes narrower while the barrier heights decrease markedly.

The effective activation energies determined from conduction vs. the inverse of temperature curves is generally used to evaluate barrier heights.[44] On the other hand, it is known that the amount of adsorbed oxygen species depends on temperature.[7] During the heating processes in air and CO, the barrier height changes as a consequence of the oxygen and CO adsorption/desorption equilibrium and of the diffusion into/out of the grains (at temperatures higher than 280 °C), and CO reactions, as it was reported in previous works.[38,40–47] However, in order to compare, the activation energies for vacuum, air and CO exposure can be estimated considering the activated process shown in Eq. (7) where only thermionic currents are considered.

Fig. 7 shows the resistance as a function of temperature when samples were cooled in vacuum, air or CO atmospheres. These curves were extracted from the cooling processes in Fig. 3. Using Eq. (9), and considering a donor concentration value of $N_d = 3.5 \times 10^{25}\ m^{-3}$, assumed by Muralt et al. (and previously reported by Kafadaryan et al. as $\approx 2.4 \times 10^{25}\ m^{-3}$)[13,45] a permittivity $\varepsilon_r = 100$ (as reported by Thomas et al.[47] for higher amounts of CuO segregated at the grain boundaries and thick films of CCTO), a barrier height of $\phi = 0.32$ eV (Fig. 7) in vacuum atmosphere and a barrier width of $\Lambda = 10$ nm were found. From this barrier width value, it is possible to consider that

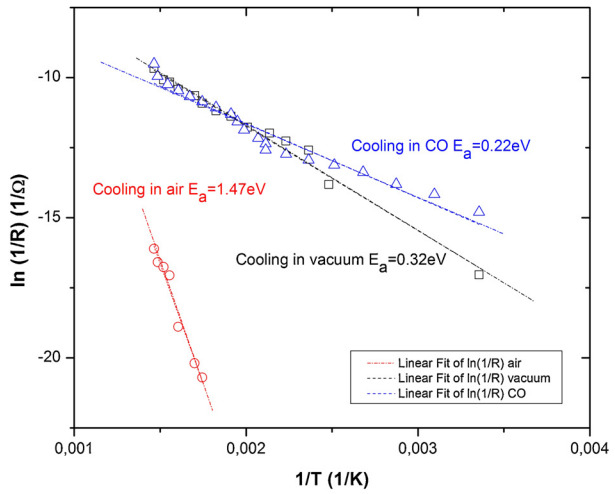

Fig. 7. Conductance (1/resistance) as a function of 1/temperature (1/T) when samples were cooled in vacuum (cycle a), air (cycle b) or CO atmospheres (cycle c).

all grains with a mean size greater than ≈100 nm, will present non-overlapped potential barriers.

Other authors also used the R vs. 1/T curves for the evaluation of the activation energies when films are exposed to different atmospheres. Table 1 shows the barrier width results for the different atmospheres. For vacuum, $E_a = \phi$, and considering that grain sizes are bigger than 100 nm (according to SEM observations), most of the grains have initially non-overlapped potential barriers. Also, for the sake of comparison, the effective activation energies reported in Table 1 show, qualitatively, the direction of barrier height changes when films are exposed to oxidizing (air) or reducing (CO) atmospheres. Moreover, due to the adsorption/desorption processes discussed above, the presence of non-parabolic potential barriers and the possible contribution from tunneling currents; those results are unreliable.[11,12,46–51] Only for vacuum cycles we can be sure that $E_a = \phi$, therefore only measurements performed in vacuum should be used. The resulting conduction vs. 1/temperature curves cannot be explained just by considering the thermionic contribution to conductivity, in which only the barrier height is relevant.

In order to improve barrier height and depletion layer calculations in vacuum, the current densities should be determined including both thermionic and tunneling contributions. In our films, if the doping is reduced (for classical model, Eq. (7)), the thermionic contribution is not affected. In contrast, the tunneling contribution is reduced as the intergranular barrier becomes wider, increasing the film resistance (Eqs. (12) and (13)). Furthermore, if the amount of oxygen diffusion into the grains is high enough (temperatures above 250 °C), the resistance will increase as a consequence of the annihilation of oxygen vacancies (N_d decreasing). At low donor concentrations, a higher permittivity value is also responsible for widening the depletion layer even more, with the resistance increasing accordingly. We considered that this dependency could be a consequence of the influence of the tunnel current in polycrystalline CCTO. The total electron current density through a potential barrier was calculated as:

$$J = J_{therm} + J_{tunnel} \tag{12}$$

where J_{therm} and J_{tunnel} are the current densities from thermionic and tunneling conduction, respectively. These currents can be expressed as:

$$J = AT^2 \exp\left[\frac{-(\phi + \xi)}{kT}\right] + \frac{AT}{k}\int_0^{\phi} F(E)P(E)dE \tag{13}$$

The first term in Eq. (13) corresponds to the thermionic contribution and the second term to the tunneling contribution. $F(E)$ is the Fermi–Dirac distribution and $P(E)$ is the transmission probability that can be calculated by means of the Wentzel–Kramer–Brillouin (WKB) approximation, and ξ the difference between the bottom of the conduction band and the Fermi level.[52] As proposed by Kafadaryan et al.[45] a value of 0.6 for the relative electron mass of CCTO was used in the calculations.

With the purpose of improving the barrier height value obtained with the E_a measurements a mathematical model using Eqs. (9), (12) and (13) was developed. Table 2 shows the calculated tunneling and thermionic current densities, the total experimental and calculated currents, and depletion layer width obtained by fitting only the vacuum experimental results of Fig. 7, using the mathematical model for tunnel plus thermionic currents and assuming a donor density of 3.5×10^{25} m^{-3} and a permittivity $\varepsilon_r = 100$. Under these conditions, the barrier height value obtained from fitting the theoretical curve was $\phi = 0.405$ eV.

Table 1
Depletion layer width (Λ) and thermionic currents as a function of activation energies obtained from Fig. 7, $N_d = 3.5 \times 10^{25}$ m^{-3} and $\varepsilon_r = 100$.

Atmosphere	E_a (eV)	T (K)	$J_{\text{Thermionic}}$ (A/m^2)	Λ ($\times 10^{-9}$ m)
CO	0.22	297	1.53×10^{-9}	8.3
		465	5.42×10^{-8}	
		685	4.72×10^{-7}	
Vacuum	0.32	297	3.52×10^{-11}	10.0
		465	5.1×10^{-9}	
		685	9.92×10^{-8}	
Air	1.47	571	1.22×10^{-13}	21.5
		621	1.47×10^{-12}	
		685	2.12×10^{-11}	

Table 2
Experimental, thermionic, tunnel and total current densities obtained by fitting the vacuum experimental results, assuming a donor density of 3.5×10^{25} m^{-3}. A barrier height of 0.405 eV and a depletion layer width (Λ) of 11.3×10^{-9} m was obtained with tunnel plus thermionic model.

T (K)	$J_{experimental}$ (A/m^2)	J_{total} simulated (A/m^2)	J_{tunnel} (A/m^2)	$J_{thermionic}$ (A/m^2)	Λ ($\times 10^{-9}$ m)	$E_a = \Phi$ (eV)
297	0.0004	0.0004	3.9×10^{-4}	8×10^{-6}		
403	0.011	0.010	0.0094	6×10^{-4}		
448	0.047	0.026	0.024	0.0021		
467	0.062	0.038	0.034	0.0034	11.3	0.405
497	0.077	0.063	0.057	0.0063		
571	0.182	0.184	0.16	0.024		
641	0.384	0.412	0.34	0.07		
685	0.625	0.631	0.51	0.12		

3.4. Time response

In Fig. 4 the time response of CCTO film when exposed to an atmosphere changing from vacuum to dry air at different temperatures is presented. The electrical resistance increases with air exposure due to the electron transfer from the n-type semiconducting material to chemisorbed oxygen on the grain surfaces.[47] Resistance versus time curves can be understood by considering that intergranular potential barriers are responsible for the observed electrical response. When samples are exposed to air a rapid increase in resistance is observed, indicating that equilibrium at the surface is quickly reached. The interaction of oxygen with grain surfaces produces the transfer of electrons from the bulk to the surface. From this process, both ϕ and Λ become larger and, as a consequence, the sample resistance increases.

For measurements carried out at 275 and 350 °C, when the atmosphere was changed from vacuum to air, an increase of the electrical resistance is observed, but for sensors exposed to air at 400 °C, the continuous, slow changes in the resistance observed after a quick initial change can be explained in terms of oxygen in-diffusion. As it was shown in a previous work, the phenomenon of annihilation of oxygen vacancies is responsible for the slow resistance decrease after the quick initial response.[39] For CCTO samples at high temperatures, the oxygen in-diffusion process is favored, annihilating oxygen vacancies in all the grains. The slow decrease of the resistance (observed at ≈650 s) is produced as a consequence of the change in doping level, N_d. As shown in SEM observations, some of the grains have sizes greater than 500 nm. This small number of grains continues with non-overlapped barriers until oxygen in-diffusion takes place. The remaining oxygen vacancies are then annihilated and a decrease of the doping level, N_d, is produced.[53,54]

4. Conclusions

CCTO thick films obtained by the screen printing technique and thermally processed at temperatures under 500 °C are suitable for application as gas sensors. CuO plays a very important role in the n-type semiconductor behavior. Due to the great permittivity range for CCTO, and different grain sizes, it is necessary to consider the possible overlapping of potential barriers due to oxygen in-diffusion when samples are exposed to air atmosphere at temperatures close to 400 °C. This phenomenon modifies the tunnel currents and due to J_{tunnel} dependence of N_d, for potential barrier height estimation it is necessary to consider that during the air exposure the barrier changes its height and width. An approximate value of ϕ can be obtained from $ln(G)$ vs. the inverse of temperature ($1/T$) only during the vacuum cooling process. The response of CCTO thick films to CO exposure is a decrease in the resistance. Initial resistance is recovered when the sample is cycled during CO exposure, indicating a reversible reaction. For further refinements in the analysis of gas sensors, tunnel currents, non-parabolic barriers, overlapped and non-overlapped barriers, and the barrier height dependence on temperature when samples are treated in different atmospheres should be considered.

Acknowledgements

This work was partially supported by the ANPCyT (Agencia Nacional de Promoción Científica y Tecnológica, Argentina), CNPq (Conselho Nacional de Desenvolvimento Científico e Tecnológico, Brasil) and CAPES (Coordenação de Aperfeiçoamento ao Pessoal de Ensino Superior, Brasil).

References

1. Neri G, Bonavita A, Micali G, Rizzo G, Callone E, Carturan G. Resistive CO gas sensors based on In_2O_3 and InSnO*x* nanopowders synthesized via starch-aided sol–gel process for automotive applications. *Sens Actuators B* 2008;**132**:224–33.
2. Epifani M, Helwig A, Arbiol J, Díaz R, Francioso L, Siciliano P, et al. TiO_2 thin films from titanium butoxide: synthesis, Pt addition, structural stability, microelectronic processing and gas-sensing properties. *Sens Actuators B* 2008;**130**:599–608.
3. Parra R, Savu R, Ramajo LA, Ponce MA, Varela JA, Castro MS, et al. Sol–gel synthesis of mesoporous $CaCu_3Ti_4O_{12}$ thin films and their gas sensing response. *J Solid State Chem* 2010;**183**:1209–14.
4. Giberti A, Carotta MC, Malagù C, Aldao CM, Castro MS, Ponce MA, et al. Permittivity measurements in nanostructured TiO_2 gas sensors. *Phys Status Solidi A* 2011;**208**:118–22.
5. Yamazoe N. Toward innovations of gas sensor technology. *Sens Actuators B* 2005;**108**:2–14.
6. Bârsan N, Hübner M, Weimar U. Conduction mechanisms in SnO_2 based polycrystalline thick film gas sensors exposed to CO and H_2 in different oxygen backgrounds. *Sens Actuators B* 2011;**157**:510–7.
7. Bârsan N, Weimar U. Conduction model of metal oxide gas sensors. *J Electroceram* 2001;**7**:143–67.
8. Cukrov LM, McCormick PG, Galatsis K, Wlodarski W. Gas sensing properties of nanosized tin oxide synthesised by mechanochemical processing. *Sens Actuators B* 2001;**77**:491–5.

9. Madou MJ, Morrison R. *Chemical Sensing with Solid State Devices*. San Diego: Academic Press Inc.; 1989. ISBN-9780323139854.
10. Bueno PR, Ramírez MA, Varela JA, Longo E. Dielectric spectroscopy analysis of $CaCu_3Ti_4O_{12}$ polycrystalline system. *Appl Phys Lett* 2006;**89**:191117.
11. Barsan N, Koziej D, Weimar U. Metal oxide-based gas sensor research: how to? *Sens Actuators B* 2007;**121**:18–35.
12. Kim II D, Rothschild A, Hyodo T, Tuller HL. Microsphere templating as means of enhancing surface activity and gas sensitivity of $CaCu_3Ti_4O_{12}$ thin films. *Nano Lett* 2006;**6**:193–8.
13. Deng G, Muralt P. Annealing effects on electrical properties and defects of $CaCu_3Ti_4O_{12}$ thin films deposited by pulsed laser deposition. *Phys Rev B* 2010;**81**:224111.
14. Deng G, He Z, Muralt P. Physical aspects of colossal constant material $CaCu_3Ti_4O_{12}$ thin films. *J Appl Phys* 2009;**105**:084106.
15. Ramirez MA, Simões AZ, Felix AA, Tararam R, Longo E, Varela JA. Electric and dielectric behavior of $CaCu_3Ti_4O_{12}$-based thin films obtained by soft chemical method. *J Alloys Compd* 2011;**509**:9930–3.
16. Sinclair DC, Adams TB, Morrison FD, West AR. $CaCu_3Ti_4O_{12}$: one-step internal barrier layer capacitor. *Appl Phys Lett* 2002;**80**:2153–5.
17. Joanni E, Savu R, Bueno PR, Longo E, Varela JA. *P*-type semiconducting gas sensing behaviour of nanoporous rf sputtered $CaCu_3Ti_4O_{12}$ thin films. *Appl Phys Lett* 2010;**92**:132110.
18. Chung SY, Kim ID, Kang SJL. Strong nonlinear current–voltage behavior in perovskite-derivative calcium copper titanate. *Nat Mater* 2004;**3**:774–8.
19. Capsoni D, Bini M, Massarotti V, Chiodelli G, Mozzati MC, Azzoni C. Role of doping and CuO segregation in improving the giant permittivity of $CaCu_3Ti_4O_{12}$. *J Solid State Chem* 2004;**177**:4494–500.
20. Bueno PR, Tararam R, Parra R, Joanni E, Ramírez MA, Ribeiro WC, et al. A polaronic stacking fault defect model for $CaCu_3Ti_4O_{12}$ material: an approach for the origin of the huge dielectric constant and semiconducting coexistent features. *J Phys D: Appl Phys* 2009;**42**:055404.
21. Fiorenza P, Lo Nigro R, Sciuto A, Delugas P, Raineri V, Toro RG, et al. Perovskite $CaCu_3Ti_4O_{12}$ thin films for capacitive applications: From the growth to the nanoscopic imaging of the permittivity. *J Appl Phys* 2009;**105**:061634.
22. Ramírez MA, Bueno PR, Varela JA, Longo E. Non-Ohmic and dielectric properties of a $Ca_2Cu_2Ti_4O_{12}$ polycrystalline system. *Appl Phys Lett* 2006;**89**:212102.
23. Ramírez MA, Bueno PR, Longo E, Varela JA. Conventional and microwave sintering of $CaCu_3Ti_4O_{12}$/$CaTiO_3$ceramic composites: non-ohmic and dielectric properties. *J Phys D: Appl Phys* 2008;**41**:152004.
24. Valim D, Souza Filho AG, Freire PTC, Fagan SB, Ayala AP, Mendes Filho JA, et al. Raman scattering and X-ray diffraction studies of polycrystalline $CaCu_3Ti_4O_{12}$ under high-pressure. *Phys Rev B* 2004;**70**:132103.
25. Amaral F, Costa LC, Valente MA, Fernandes AJS, Franco N, Alves E, et al. Colossal dielectric constant of poly- and single-crystalline $CaCu_3Ti_4O_{12}$ fibres grown by the laser floating zone technique. *Acta Mater* 2011;**59**:102–11.
26. Mageshwari K, Sathyamoorthy R. Flower-shaped CuO nanostructures: synthesis, characterization and antimicrobial activity. *J Mater Sci Technol* 2013;**29**(10):909–14.
27. Xu JF, Ji W, Shen ZX, Li WS, Tang SH, Ye XR, et al. Raman spectra of CuO nanocrystals. *J Raman Spectrosc* 1999;**30**:413–5.
28. Ohsaka T, Izumi F, Fujiki Y. Raman spectrum of anatase, TiO_2. *J Raman Spectrosc* 1978;**7**(6):321–4.
29. Oliveira LH, de Moura AP, Mazzo TM, Ramírez MA, Cavalcante LS, Antonio SG, et al. Structural refinement and photoluminescence properties of irregular cube-like $(Ca_{1-x}Cu_x)TiO_3$ microcrystals synthesized by the microwave hydrothermal method. *Mater Chem Phys* 2012;**136**:130–9.
30. Yu R, Xue H, Cao Z, Chen L, Xiong Z. Effect of oxygen sintering atmosphere on the electrical behavior of CCTO ceramics. *J Eur Ceram Soc* 2012;**32**:1245–9.
31. Ramirez MA, Bueno PR, Tararam R, Cavalheiro AA, Longo E, Varela JA. Evaluation of the effect of the stoichiometric ratio of Ca/Cu on the electrical and microstructural properties of the $CaCu_3Ti_4O_{12}$ polycrystalline system. *J Phys D: Appl Phys* 2009;**42**:185503.
32. Yeoh CK, Ahmad MF, Ahmad ZA. Effects of Cu and Ti excess on the dielectric properties of $CaCu_3Ti_4O_{12}$ prepared using a wet chemical method. *J Alloys Compd* 2007;**443**:155–60.
33. Fang TT, Mei LT. Evidence of Cu deficiency: a key point for the understanding of the mystery of the giant dielectric constant in $CaCu_3Ti_4O_{12}$. *J Am Ceram Soc* 2007;**90**:638–40.
34. Shao SF, Zhang JL, Zheng P, Wang CL. Effect of Cu-stoichiometry on the dielectric and electric properties in $CaCu_3Ti_4O_{12}$ ceramics. *Solid State Commun* 2007;**142**:281–6.
35. Mei LT, Hsiang HI. Effect of copper-rich secondary phase at the grain boundaries on the varistor properties of $CaCu_3Ti_4O_{12}$ ceramics. *J Am Ceram Soc* 2008;**91**:3735–7.
36. Foschini CR, Tararam R, Simões AZ, Cilense M, Longo E, Varela JA. $CaCu_3Ti_4O_{12}$ thin films with non-linear resistivity deposited by RF-sputtering. *J Alloys Compd* 2013;**574**:604–8.
37. Zhang Q, Li T, Chen Z, Xue R, Wang Y. The non-ohmic and dielectric behavior evolution of $CaCu_3Ti_4O_{12}$after heat treatments in oxygen-rich atmosphere. *Mater Sci Eng B* 2012;**177**:168–72.
38. Ponce MA, Castro MS, Aldao CM. Influence of oxygen adsorption and diffusion on the overlapping of intergranular potential barriers in SnO_2 thick films. *Mater Sci Eng B* 2004;**111**:14–9.
39. Blaustein G, Castro MS, Aldao CM. Influence of frozen distributions of oxygen vacancies on tin oxide conductance. *Sens Actuators B* 1999;**55**: 33–7.
40. Ponce MA, Malagù C, Carotta MC, Martinelli G, Aldao CM. Gas indiffusion contribution to impedance in tin oxide thick films. *J Appl Phys* 2008;**104**:054907.
41. Romppainen P, Lantto V. The effect of microstructure on the height of potential energy barriers in porous tin dioxide gas sensors. *J Appl Phys* 1988;**63**:5159–65.
42. Sahm T, Gurlo A, Barsan N, Weimar U. Basics of oxygen and SnO_2 interaction work function change and conductivity measurements. *Sens Actuators B* 2006;**118**:78–83.
43. Crowell CR, Rideout VL. Normalized thermionic-field (T-F) emission in metal-semiconductor (Schottky) barriers. *Solid State Electron* 1969;**12**:89–105.
44. Kim D, Rothschild A, Tuller H. Direct current bias effects on grain boundary Schottky barriers in $CaCu_3Ti_4O_{12}$. *Appl Phys Lett* 2006;**88**:072902.
45. Kafadaryan EA, Cho K, Wu N. Far-infrared study of high-dielectric constant $CaCu_3Ti_4O_{12}$ films. *J Appl Phys* 2004;**96**:6591–6.
46. Thomas P, Dwarakanath K, Varma KBR. Effect of calcium stoichiometry on the dielectric response of $CaCu_3Ti_4O_{12}$ ceramics. *J Eur Ceram Soc* 2012;**32**:1681–90.
47. Schipani F, Aldao C, Ponce M. Schottky barriers measurements through Arrhenius plots in gas sensors based on semiconductor films. *AIP Adv* 2012;**2**:032138.
48. Li J, Sleight AW, Subramanian MA. Evidence for internal resistive barriers in a crystal of the giant dielectric constant material: $CaCu_3Ti_4O_{12}$. *Solid State Commun* 2005;**135**:260–2.
49. Izydorczyk W. Numerical analysis of an influence of oxygen adsorption at a SnO_2 surface on the electronic parameters of the induced depletion layer. *Phys Status Solidi B* 2011;**248**:694–9.
50. Aldao C, Malagù C. Non-parabolic intergranular barriers in tin oxide and gas sensing. *J Appl Phys* 2012;**112**:024518.
51. Aldao CM, Mirabella DA, Ponce MA, Giberti A, Malagù C. Role of intragrain oxygen diffusion in polycrystalline tin oxide conductivity. *J Appl Phys* 2011;**109**:063723.
52. Ponce MA, Ramírez MA, Parra R, Malagu C, Castro MS, Bueno PR, et al. Influence of degradation on the electrical conduction process in ZnO and SnO_2-based varistors. *J Appl Phys* 2010;**108**:074505.
53. Malagù C, Giberti A, Morandi S, Aldao C. Electrical and spectroscopic analysis in nanostructured SnO2: "Long-term" resistance drift is due to in-diffusion. *J Appl Phys* 2011;**110**:093711.
54. Kamp B, Merkle R, Maier J. Chemical diffusion of oxygen in tin dioxide. *Sens Actuators B* 2001;**77**:534–42.